Processing-dependent intracrystallite and intercrystallite structuring and charge transport in poly(3-hexylthiophene)

Kaichen Gu¹, Yucheng Wang¹, Ruipeng Li², Esther Tsai³, Jonathan W. Onorato⁴, Christine K. Luscombe^{4,5,6}, Rodney D. Priestley^{1,7}, and Yueh-Lin Loo^{1,8}

Keywords: Conjugated polymers, polymer tie chains, Field-effect transistors, Organic electronics, Charge transport

Corresponding Author

* E-mail: <u>lloo@princeton.edu</u>

¹ Department of Chemical and Biological Engineering, Princeton University, Princeton, New Jersey 08544, United States

² National Synchrotron Light Source II (NSLS II), Brookhaven National Laboratory, Upton, New York, 11973, United States.

³ Center for Functional Nanomaterials, Brookhaven National Laboratory, Upton, New York, 11973, United States.

⁴ Materials Science and Engineering Department, University of Washington, Seattle, WA 98195-2120, United States

⁵ Department of Chemistry, University of Washington, Seattle, WA 98195-1700, United States

⁶ Molecular Engineering & Sciences Institute, University of Washington, Seattle, WA 98195, United States

⁷ Princeton Institute for the Science and Technology of Materials, Princeton University, Princeton, New Jersey 08544, United States

⁸ Andlinger Center for Energy and the Environment, Princeton University, Princeton, New Jersey 08544, United States

Abstract

The performance of electronic devices comprising conjugated polymers as the active layer depends not only on the intrinsic characteristics of the materials but also on the details of the extrinsic processing conditions. In this study, we examine the effect of postdeposition thermal treatments on the microstructure of poly(3-hexylthiophene) (P3HT) thin films and its impact on their electrical properties. We find thermal annealing of P3HT thin films to generally increase their crystallinity and crystallite coherence length while retaining the same crystal structure. Despite such favorable structural improvements of the polymer active layers, thermal annealing at high temperatures can lead to a net reduction in the mobility of transistors, implicating critical changes in the intercrystallite structure that are not accounted for in the simplistic picture that crystallinity governs charge transport. Our results suggest tie-chain pull-out, which occurs during crystal growth and perfection upon thermal annealing to be responsible. By demonstrating the interplay between intracrystallite and intercrystallite structuring in determining the macroscopic charge transport, we shed light on understanding how processing conditions can impact charge-transport properties for the same polymer material.

Introduction:

Conjugated semiconducting polymers have demonstrated great potential as active layers in next-generation electronic devices that are low-cost, lightweight, and flexible. 1,2 Through iterations and refinement on the design of new materials and optimization of processing conditions, the research community has drastically improved the performance of conjugated-polymer-based devices, with reported mobilities of field-effect transistors comprising them routinely above 1 cm² V⁻¹ s⁻¹, ^{3,4} and power-conversion efficiencies of solar cells above 15%. 5,6 The performance of electronic devices comprising conjugated polymers depends strongly on their intrinsic materials characteristics, including molecular weight and molecular weight distribution, regioregularity, and chain rigidity, and also on the details of extrinsic processing conditions. ⁷⁻¹⁰ Owing to the conformational freedom of polymer chains and the weak intermolecular forces that govern their structuring, the solid-state morphology of solution-processed polymers is directly impacted by the specifics of processing conditions, including the choice of solvent from which the polymer is processed, 11,12 solution engineering by sonication and aging, ^{13–15} casting techniques and details, ^{16,17} as well as post-deposition thermal ^{18–20} and solvent-vapor annealing treatments.^{21,22} The microstructural differences in turn impact charge transport. It has been demonstrated in many conjugated polymers, including poly(3-hexylthiophene) (P3HT),²³ poly[4-(4,4-dihexadecyl-4*H*-cyclopenta[1,2-b:5,4b']dithiophen-2-yl)-alt-[1,2,5]thiadiazolo-[3,4-c]pyridine] (PCDTPT), 24,25 and poly[2,6-(4,4-bis-alkyl-4*H*-cyclo-penta-[2,1-b;3,4-b0]-dithiophene)-*alt*-4,7-(2,1,3benzothiadiazole)] (CDTBTZ), ^{25,26} that the mobility of transistors comprising the same polymer can vary by more than an order of magnitude depending on how the active layer is processed.

Such dependence of charge-transport properties on processing conditions renders *a priori* predictions of electrical properties from the chemical structure of polymers extremely challenging.^{27,28} Understanding how processing conditions impact the microstructure of conjugated polymers will allow us to devise methods of controlling the microstructure and accordingly facilitate the reproducible access of microstructures that give rise to desired electrical properties. Prior work has shown the thermal history of conjugated

polymers to strongly impact their microstructure development. ^{18,19,29} While thermal annealing is generally thought to improve polymer crystallinity by crystallite thickening, its impact on the intercrystallite amorphous region is less studied in part because of the difficulties associated with visualizing and characterizing amorphous, but chemically-identical polymer chains. ³⁰ In this work, we systematically investigate the structural and electrical property changes of thin films of model P3HT induced by post-deposition annealing to develop insights on the role of the intercrystallite structuring in impacting charge transport. We are particularly interested in understanding the effects of tie chains, long polymer chains that bridge neighboring crystallites and thus provide electrically-connective pathways between them, on charge transport. ^{31,32} Previously, we found that connectivity between neighboring crystallites to be crucial for macroscopic charge transport in P3HT, and percolation sets in when the tie-chain fraction is above 10⁻³, as quantified by the Huang-Brown model. ³³

Here, we judiciously selected two P3HT samples that have distinct tie-chain fractions, quiescently crystallized P3HT 40 has a tie-chain fraction of 6×10⁻³ while P3HT 5/40 has a tie-chain fraction of 9×10^{-5} . These samples were chosen because their tie-chain fractions put P3HT 40 above and P3HT 5/40 below the percolation threshold for developing macroscopic charge-transport networks.³³ Comparing the processingstructure-property relationships of these two samples will allow us to gain insight into how intercrystallite connectivity contributes to the processing-dependent charge transport in P3HT. We find thermal annealing to generally increase crystallinity and crystallite coherence length of the polymer active layers, with P3HT retaining the same crystal structure across all processing conditions. Despite such favorable structural improvements of the polymer active layers, thermal annealing at high temperatures can lead to a net reduction in the mobility of transistors. This effect, which we surmise to result from the pull-out of tie chains upon thermal annealing, is more pronounced in transistors comprising sub-percolative P3HT 5/40 compared to those comprising percolated P3HT 40. We take this observation to indicate the importance of intercrystallite connectivity, highlighting the adverse role of tie-chain pull-out upon thermal annealing on charge transport.

Results and Discussion:

We fabricated field-effect transistors comprising P3HT _40 and P3HT_5/40 films that had been annealed at different temperatures. All films were annealed for ten minutes at the specified temperatures. The annealing temperatures (T_a) ranged from 30 °C to 170 °C, which we chose because they span the glass transition temperature (12-14 °C)³⁴ and the melting point of P3HT (equilibrium melting temperature at 272 °C).³⁵ For completeness, we also measured the mobility of transistors with as-cast P3HT that was kept at room temperature; these are denoted with $T_a = 20$ °C. This same reference is used to denote films that were kept at room temperature for the accompanying structural studies.

Figure S1 shows the field-effect mobility of transistors as a function of the annealing temperature their active layers were subjected to. The mobility of P3HT_40 transistors is consistently higher than that of P3HT_5/40 transistors across the entire temperature range explored, in agreement with previous reports that have shown the mobility of transistors to generally increase with the molecular weight of the polymer that comprises the active layer. This trend is also consistent with our prior tie-chain fraction calculations that showed that quiescently crystallized P3HT_40 has a higher tie-chain fraction than that of P3HT_5/40, as the additional tie chains in P3HT_40 provide sufficient pathways for more efficient charge transport between neighboring crystalline domains. Despite the presence of the amorphous regions in these semicrystalline P3HT films, the mobilities of the P3HT_40 transistors are comparable to what had been reported for charge transport within individual P3HT crystallites (0.01 cm² V⁻¹ s⁻¹), suggesting the presence of a percolated network for charge transport in P3HT_40 across all the conditions explored in this study. 33,36

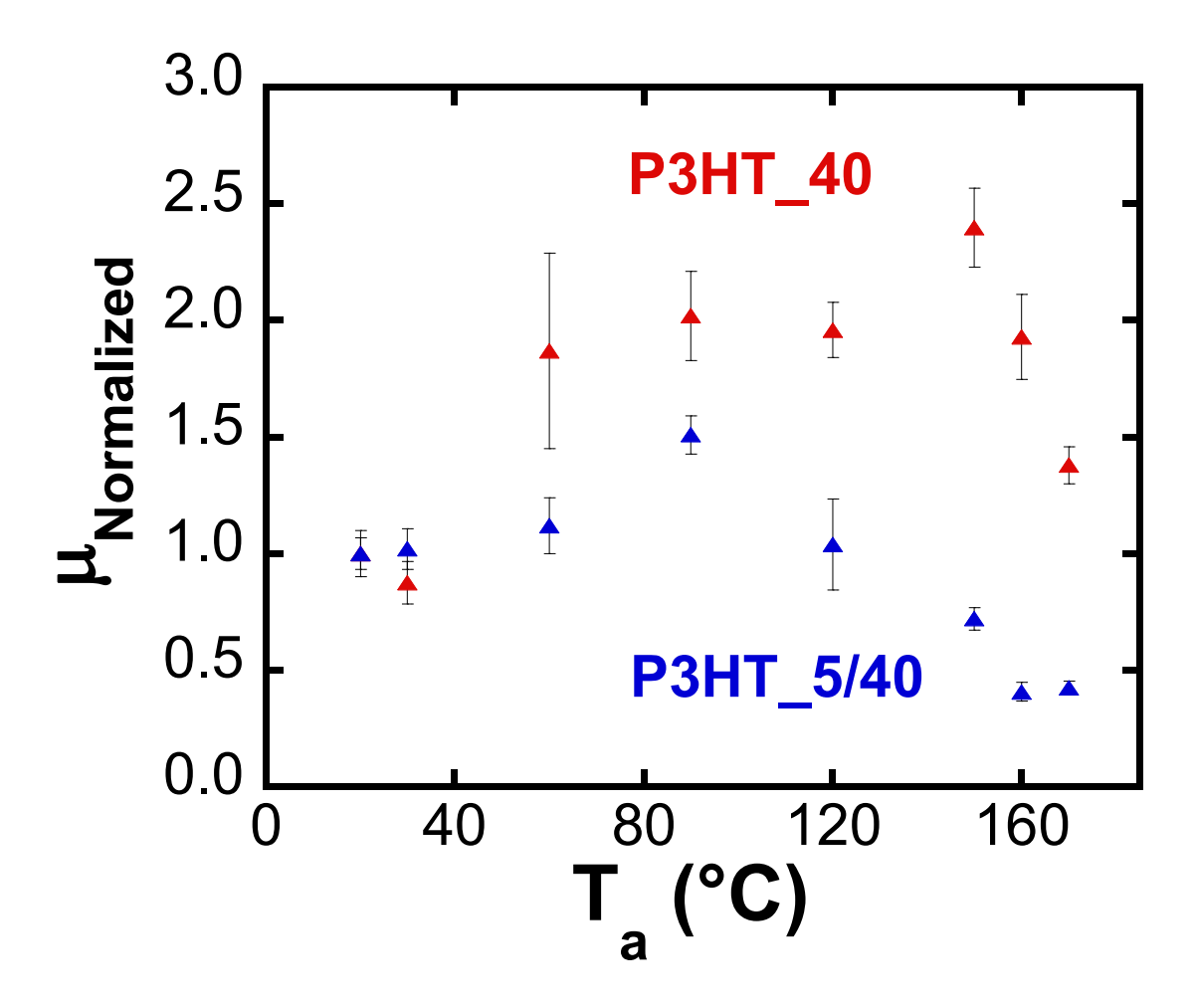


Figure 1. Normalized field-effect mobility of transistors comprising P3HT _40 and P3HT_5/40 films that had been annealed at different temperatures.

Figure 1 plots the field-effect mobilities of P3HT_40 and P3HT_5/40 transistors, normalized against the mobility of the transistor comprising the respective as-cast P3HT films. For both P3HT_40 and P3HT_5/40 transistors, the mobility first increases with annealing temperature and then drops precipitously. Since thermal annealing generally improves the crystalline order in polymer thin films, we surmise this improvement in structural order to account for the initial improvements in the mobility of these P3HT transistors on annealing. Yet, the fact that the mobility of both transistors drops substantially at higher yet annealing temperatures, above 150 °C for P3HT_40 or above 90 °C for P3HT_5/40, suggests that there are additional thermally-induced structural changes we had not accounted for in this simplistic picture that crystallinity dictates charge transport in conjugated polymer thin films. Despite this qualitatively similar trend,

subtle differences also exist between P3HT_40 and P3HT_5/40. In particular, the mobility of transistors comprising P3HT_5/40 that had been annealed above 120 °C drops by approximately half compared to that of transistors comprising as-cast P3HT_5/40, with the mobility of transistors comprising P3HT_40 always higher than that of the transistor comprising the initial, as-cast film. Conversely, the mobility of P3HT_5/40 transistors that had been annealed above 120 °C is lower than the mobility of the same transistor with an as-cast active layer. This comparison suggests that our presumed structural changes at elevated temperatures adversely affect P3HT_5/40 more than they do P3HT_40.

To understand the structural origins for the observed trend in field-effect mobilities, we investigated the microstructural changes resulting from post-deposition thermal annealing of P3HT_40 and P3HT_5/40 thin films.

We first used flash DSC to measure the thermal properties of the same P3HT samples, from which we extracted the thermal transitions and interpreted the microstructural parameters associated with P3HT crystallites.³⁵ Flash DSC has emerged as a useful tool to investigate polymer crystallization over a wide range of thermal histories efficiently, especially for fast crystallizers.^{37–39} Flash DSC has allowed us to access heating rates as high as 800 °C/s to extract thermal properties without inducing cold recrystallization that one typically encounters with standard DSC, at rates of ca. 10-20 °C/min. Figure S2a shows the temperature protocol used in this study. The flash DSC thermograms for P3HT_40 and P3HT_5/40 resulting from the same temperature protocol are shown in Figures S2b, c. From the thermograms, we obtained the melting point and the specific melting enthalpy for these semicrystalline P3HT thin films, from which we extracted the corresponding crystallite thickness and crystallinity.³⁵ Here, we have chosen to determine the crystallinity of these P3HT samples based on calorimetry experiments, as opposed to X-ray diffraction because the former is more sensitive to the presence of smaller crystallites and less sensitive to sample thickness and roughness variation than the latter.

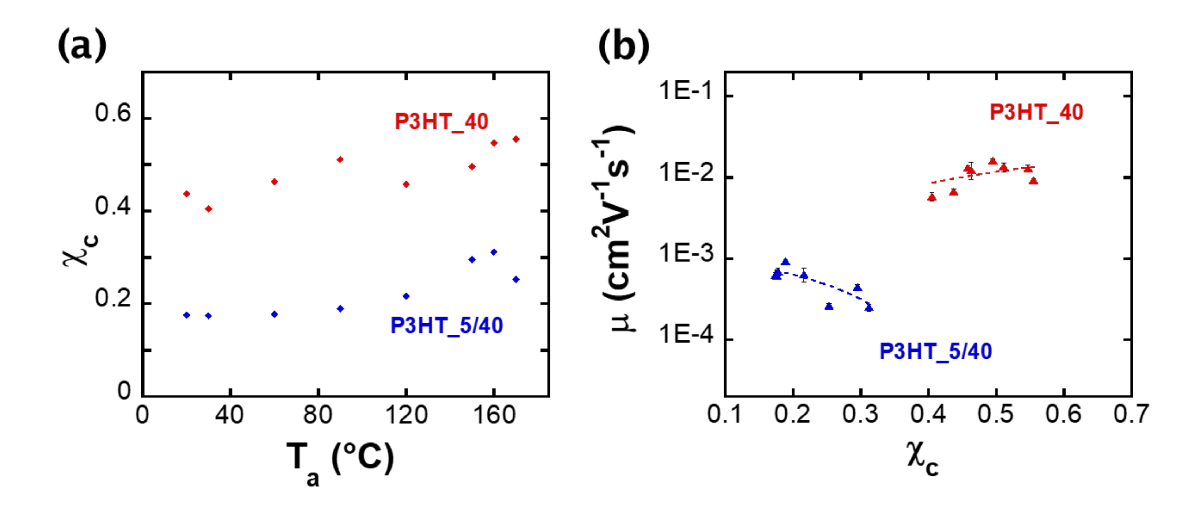


Figure 2. (a) The crystallinity, as determined from the specific melting enthalpy, of P3HT_40 and P3TH_5/40 as a function of annealing temperature. (b) The field-effect mobility of transistors comprising those films as a function of their crystallinity. The dotted lines represent the best linear fits to the mobility data.

Figures S3 tracks the crystal thickness for both P3HT_40 and P3HT_5/40. The crystallite thickness generally increases with annealing temperature. This observation is expected since post-deposition thermal annealing allows second-order structural rearrangement to take place, with thickening of crystallites to reduce their surface-to-volume ratio as a common route to accessing energetically more favorable states. 40,41

Figure 2a plots the crystallinity for both samples as a function of annealing temperature. We found the crystallinity of P3HT_40 films to be consistently higher than that of P3HT_5/40 films, irrespective of thermal history. This observation is expected because P3HT_5/40 comprises shorter chains that have a tendency to twist along its backbone, which can impede packing. This observation is also consistent with prior reports that the specific melting enthalpy generally increases with increasing molecular weight of P3HT. Additionally, the crystallinity generally increases with annealing temperature because polymer chains are more mobile at higher temperatures and can thus reorganize themselves more readily to approach their thermodynamically favorable crystalline state. **Figure 2b** shows the field-effect mobility of P3HT_40 and P3HT_5/40 films as a function of crystallinity. With the two samples, we access different ranges of

crystallinity. We found the field-effect mobility of transistors comprising P3HT_40 to increase modestly with crystallinity, which we expected because charge carriers travel faster in crystalline than in amorphous regions.⁴⁴ Interestingly, we found the field-effect mobility of transistors comprising P3HT_5/40 to decrease with increasing crystallinity, suggesting the differences in intercrystallite structuring on thermal annealing between the two polymer thin films to be responsible for the variations we observe in their electrical properties.

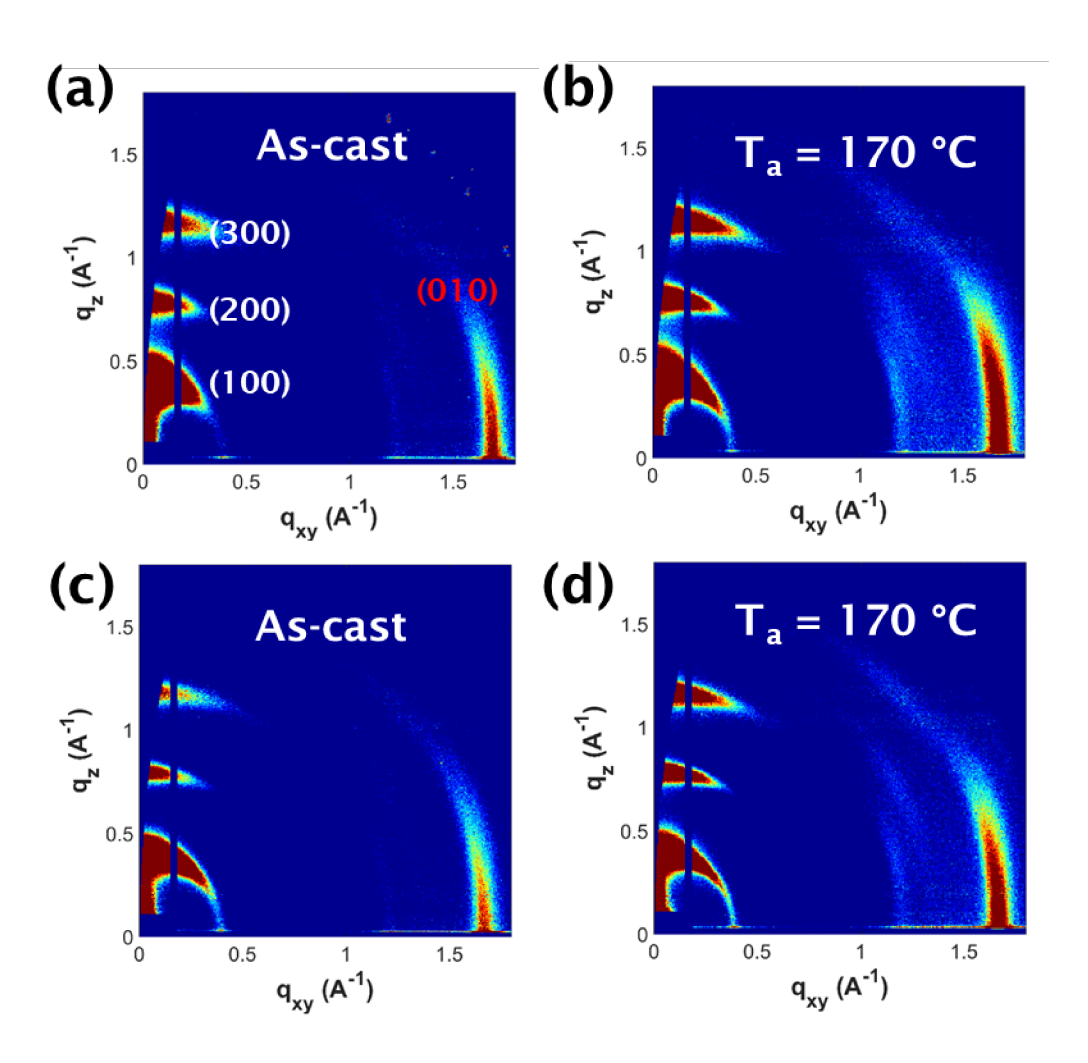


Figure 3. 2D GIXD pattern of (a) the as-cast P3HT_40 thin film and (b) the P3HT_40 thin film that had been annealed at 170 °C. 2D GIXD pattern of (c) the as-cast P3HT_5/40 thin film and (d) the P3HT_5/40 thin film that had been annealed at 170 °C. All images have been corrected for the "missing wedge" of data along the out-of-plane direction.⁴⁵

Figures 3a, b show the 2D GIXD patterns of an as-cast P3HT_40 film and one that had been annealed at 170 °C, while **Figures 3c, d** show the 2D GIXD patterns of an as-cast P3HT_5/40 film and one that had been annealed at 170 °C, respectively. The 2D GIXD patterns of P3HT_40 films and P3HT_5/40 films that had been annealed at other temperatures are shown in **Figure S4** and **Figure S5**, respectively. Regardless of the annealing temperature, the (h00) reflections of P3HT always appear on the meridian of the x-ray diffraction patterns, indicating that crystallites in P3HT_40 and P3HT_5/40 films always adopt a predominantly "edge-on" texture in which the alkyl side-chain stacking direction is normal to the substrate, with the π-stack and the polymer backbone oriented in the plane of the substrate.

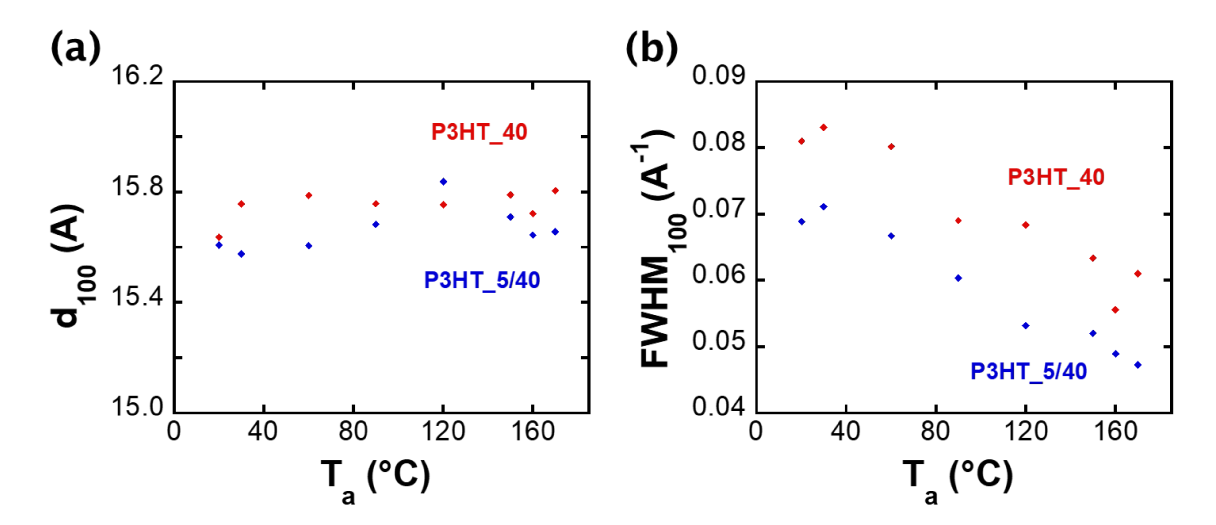


Figure 4. (a) The d-spacing of the (100) reflection, d_{100} , or the characteristic distance in the alkyl stacking direction, of P3HT_40 and P3HT_5/40 thin films as a function of annealing temperature. (b) The full peak width at half its maximum intensity of the (100) reflection, $FWHM_{100}$, of P3HT_40 and P3HT_5/40 as a function of annealing temperature. Both the d-spacing and the FWHM of the (100) reflection were extracted from the radially integrated traces of the respective 2D GIXD image.

From the radially integrated traces of the 2D GIXD images, we determined the characteristic distance along the alkyl side chain packing direction, d_{100} , and the full peak width at half its maximum intensity of the (100) reflection, $FWHM_{100}$; both quantities are summarized in **Figure** 4 as a function of annealing temperature. In both P3HT_40 and

P3HT_5/40, d_{100} is largely independent of the annealing temperature at approximately 15.7 nm (corresponding to q-vector at 0.4 Å⁻¹), which indicates that P3HT retains the same crystal structure on annealing and this crystal structure is analogous to the one that had been widely reported in the literature.⁴⁸ The $FWHM_{100}$ of the (100) reflection progressively decreases with increasing temperature, which suggests an increase in the crystallite coherence length along the alkyl side-chain packing with annealing. This observation, too, is consistent with previous study.²⁹

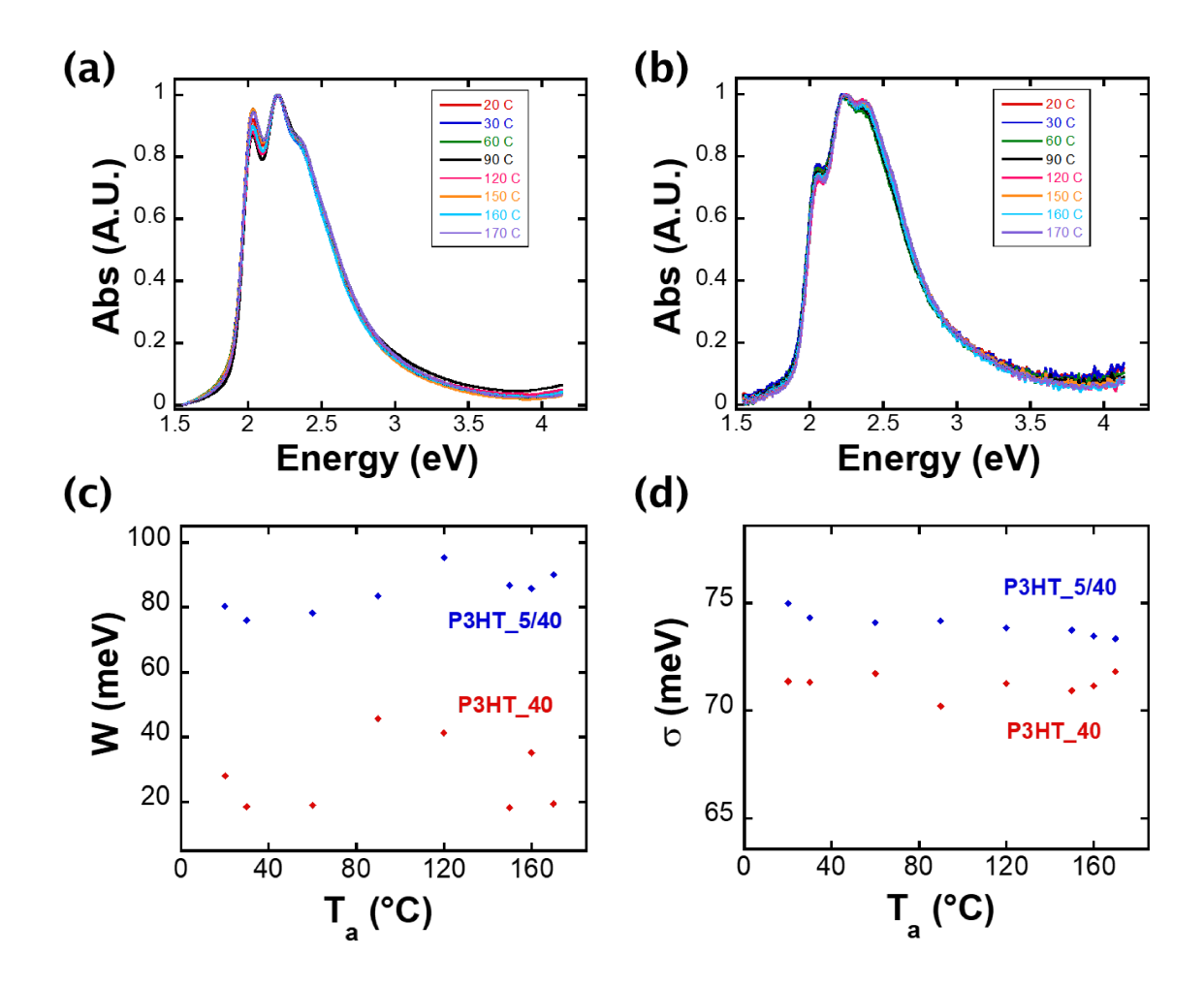


Figure 5. (a) The optical absorption spectra of (a) P3HT_40 and (b) P3HT_5/40 thin films annealed at different temperatures. These spectra were fitted with the Spano model to extract the free exciton bandwidth (W) and the Gaussian line width (σ). (c) Free exciton bandwidth and (d) Gaussian line width of P3HT_40 and P3TH_5/40 as a function of annealing temperature.

Thus far, the combination of flash DSC and GIXD has informed us of the improvements in crystallinity, crystallite thicknesses, and crystallite coherence length of P3HT thin films upon thermal annealing. To investigate the quality of ordering within crystallites, we carried out optical absorption spectroscopy of these same films. Figures 5a,b show the optical absorption spectra of P3HT 40 and P3HT 5/40 films that had been annealed at different temperatures, respectively. Qualitatively, the optical absorption spectra of P3HT 40 and P3HT 5/40 films remain largely invariant with annealing temperature. We fitted these spectra with the Spano model to extract the free exciton bandwidth (W) and the Gaussian line width (σ) , which measure the quality of ordering within P3HT aggregates. 12,49 W is inversely correlated with intrachain ordering along the backbone direction while σ is inversely correlated with the interchain ordering along the π -stacking direction. 12,50 W and σ of P3HT 40 and P3TH 5/40 as a function of annealing temperature are shown in Figures 5c,d respectively. We see that both W and σ of P3HT 40 films are consistently lower than those of P3HT 5/40 across the entire temperature range explored, suggesting both better intrachain and interchain ordering in the higher-molecular-weight thin film of P3HT 40. Our observations are consistent with previous optical measurements. 33,50,51 There is, however, no clear dependence of W on T_a in either P3HT 40 or P3HT 5/40. We interpret this observation to indicate that the ordering along the P3HT backbone is comparable in samples that were annealed at temperatures across the range of interest. σ does not vary significantly in P3HT 40 or P3HT 5/40 either, suggesting that the extent of ordering along the P3HT π -stack is also retained on annealing.

While our study implicates structural development differences on thermal annealing to be responsible for the variation in mobility of transistors of P3HT_40 and P3HT_5/40, our structural characterization – which had been focused on properties associated with P3HT crystallites – does not reveal the origin. As examples, we see that thermal annealing improves the crystallinity of P3HT active layers, but it does not necessarily lead to improved charge transport. Instead, annealing above certain temperatures, 150 °C for P3HT_40 or 90 °C for P3HT_5/40, instead hampers charge transport despite improvements in crystallinity and crystal quality. We thus surmise that differences in the structuring of the amorphous regions to be responsible for the variation in the mobility of

P3HT transistors on annealing. We further speculate that this reduction in mobility on annealing to stem from a significant reduction in the number of tie chains that provide electrical pathways between neighboring crystallite domains. Yet, the presence of tie chains in the amorphous regions – being chemically identical to the crystalline regions but structurally disordered – are notoriously challenging to characterize via conventional experimental techniques.³⁰

Previously, we had successfully quantified the tie-chain fraction of quiescently crystallized P3HT samples per the Huang-Brown framework.³³ This same framework, however, cannot be applied to quantify the tie-chain content in these thermally annealed P3HT samples. Crucial to our prior analysis is the assumption that the characteristic size of polymer chains in the melt or the solution state is preserved on rapid crystallization.⁵² This assumption is not applicable for polymers that undergo post-deposition thermal annealing given the second-order restructuring that can take place, as we have outlined above. Extended thermal annealing affords mobile polymer chains to disentangle and reorganize, and consequently, their conformation deviates substantially from their original state in the melt. The process of crystal perfection, as evidenced by crystal thickening and an increase in crystallinity, often comes at a cost of tie-chain pull-out, a process by which tie chains are drawn out of the crystallites they connect and they, along with other chains in the amorphous regions, are instead incorporated as crystalline segments as part of the growing crystallites.^{53,54} This reduction in the number of tie chains bridging crystalline domains is presumed to be responsible for the drop in mechanical toughness in polypropylene samples upon thermal annealing as the number of tie chains that can act as stress-transfer units between the crystalline domains is decreased.⁵⁴ Analogously, since tie chains electrically bridge adjacent crystalline domains to facilitate charge transport across the amorphous regions, ^{31,32} a decrease in tie-chain content upon post-deposition thermal annealing can lead to a decrease in the number of the pathways available to facilitate macroscopic charge transport in semicrystalline conjugated polymers.

Tie-chain pull-out manifests itself differently in P3HT_40 compared to P3HT_5/40; this phenomenon appears to impact the charge transport characteristics of P3HT_40 less

significantly than those of P3HT 5/40. Since macroscopic charge transport in P3HT 40 generally improves with an increase in crystallinity, we believe the tie-chain fraction of P3HT 40 – which was above the percolation threshold to begin with – to remain above the percolation threshold even after tie-chain pull-out with post-deposition thermal annealing. On the other hand, given that the tie-chain content of as-cast P3HT 5/40 is insufficient to support macroscopic charge transport to begin with, any tie-chain pull-out further decreases its ability to transport charge over macroscopic distances. Despite the simultaneous increase in crystallinity upon thermal annealing, the reduction of critical connective pathways between neighboring crystallites becomes the bottleneck to charge transport. Consistently, we see that the mobility of P3HT 5/40 transistors tend towards a limiting value of 10⁻⁴ cm² V⁻¹ s⁻¹ as crystallites in the active layers become less connected; this mobility value corresponds to that reported when the charge-transport rate associated is limited by slow interchain hopping through the amorphous region.^{33,55} The comparison between P3HT 40 and P3HT 5/40 reinforces the importance of intercrystallite connectivity and suggests that a sufficiently percolated charge-transport network is less prone to the adverse effect of tie-chain pull-out upon thermal annealing. Along these lines, long and rigid chains are preferred because they are more likely to form tie chains per the Huang-Brown model.³³

Further, the extent with which post-deposition processing affects charge-transport properties strongly depends on the deposition conditions of the polymer films, as these initial conditions determine how far the as-cast samples are away from equilibrium. For example, Turner *et al.* found both the structural development and electrical properties of P3HT films cast from dichlorobenzene solutions to be weakly affected by thermal annealing while those of the same samples cast from chloroform solutions to be strongly affected by thermal annealing because the higher boiling point of dichlorobenzene solvent allows more time for P3HT to crystallize and evolve towards the equilibrium structure and consequently the as-cast samples are less responsive to post-deposition thermal annealing.⁴⁹ This comparison again highlights the importance of a holistic approach in optimizing the charge-transport properties of conjugated polymers that considers all the combined effects of intrinsic materials properties, deposition conditions,

as well as post-deposition treatments. The effect of microstructure on charge transport is multifaceted and cannot be easily reduced to any single structural parameter.⁸

Conclusions

We have examined the molecular packing and mesoscale structure of P3HT films that had been annealed at different temperatures. We found that thermal annealing can generally increase crystallinity and the crystallite coherence length of the polymer active layer. Yet, annealing P3HT at high temperatures can impede charge transport, implicating critical changes in intercrystallite structuring. Our data suggest tie-chain pull-out, which happens during crystal growth and perfection upon thermal annealing to be responsible. The extent with which tie-chain pull-out hampers charge transport depends on the initial quiescent tie-chain content of the samples; such a detrimental effect is more pronounced in sub-percolated P3HT_5/40 than the percolated P3HT_40. As the crystallites in P3HT_5/40 become even less interconnected, the mobility of respective transistors continually decreases, approaching the value associated with charge transport through interchain hopping in the amorphous regions, in the absence of any intercrystallite connectivity.

Through investigating the changes in the microstructure and charge-transport properties of P3HT on post-deposition thermal annealing, we have demonstrated the complex interplay of crystallinity, intracrystallite ordering, and intercrystallite connectivity on determining the macroscopic charge transport in conjugated polymers. Our findings shed light on understanding how processing conditions can impact charge-transport properties for the same polymer material.

Experimental methods

Materials: All solvents were purchased from Fisher Scientific and used as-received. ⁵⁶ Hexamethyldisilazane (HMDS) was purchased from Sigma Aldrich and used as-received. P3HT was synthesized per literature, resulting in tolyl-group initiated 100% regionegular P3HT. ^{57,58} P3HT_40 has a number-average molecular weight (M_n) of 40 kg mol⁻¹ and dispersity (D) of 1.27, and P3HT_5 has M_n of 5 kg mol⁻¹ and D of 1.26, as determined in

our previous study.⁵⁸ P3HT_5/40 in this study refers to the homopolymer blend of P3HT 5 and P3HT 40 with the weight fraction of P3HT 40 to be 0.25.

Transistor Fabrication and Characterization: All thin-film transistors were fabricated in a bottom-gate-top-contact manner. Si (100) wafers with 300 nm thermally-grown SiO₂ (purchased from Process Specialties, Inc.) were used as gate and gate dielectric, respectively. The substrates were cleaned by sonication in deionized water, acetone, isopropanol for 5 minutes each, and then dried with nitrogen stream. Their oxide surfaces were modified by spin-coating HMDS at 1800 rpm, followed by thermal annealing at 120 °C for 5 min. P3HT was drop-casted (0.5 mg/mL solution in chloroform) onto the substrates at ambient conditions. 50 nm of gold was then thermally evaporated onto the substrates at a rate of ≈1.0 A s⁻¹, through a stencil mask to define active channels with a width of 204 μm and a channel length of 50 μm. All transistors were tested under vacuum using an Agilent 4155C semiconductor parameter analyzer. The hole mobilities were estimated in the saturation regime at a source-drain voltage of -80 V.

Thermal characterization: Flash DSC measurements were conducted with a Mettler-Toledo chip calorimeter from (Flash DSC 1). The Flash DSC1 was connected to an IntraCooler and nitrogen was used as the purge gas. The temperature calibration was performed using indium. The chip sensors were conditioned and corrected before use. To mimic the crystallization kinetics of depositing the polymer active layer as described above (the drying time was approximately 50 s), the sample was cooled from the melt at 270 °C to 20 °C at a rate of 5 °C/s before post-deposition thermal annealing. To extract the melting enthalpies, the sample was heated from the melt at 20 °C to 270 °C at a rate of 800 °C/s. The infinitesimal sample mass on the chip sensor needs to be determined for quantifying the specific melting enthalpies. With this purpose, each sample was also cooled from the melt at 270 °C to 20 °C at a rate of 10 °C/min, the same rate as that used in the standard DSC measurements. By assuming the same crystallization protocol leads to the same crystallinity, reflected by the same specific melting enthalpy, ⁵⁹ the effective sample mass on the flash DSC chip sensor was estimated by dividing the flash-DSCmeasured melting enthalpy by the regular-DSC-measured specific melting enthalpy that had been obtained in our prior study.³³

Optical absorption Measurements: P3HT thin films were drop-casted onto precleaned glass slides in the same manner as described above. Absorption spectra were recorded using an Agilent Technologies Cary 5000 spectrophotometer.

Grazing-Incidence X-Ray Diffraction: P3HT thin films for GIXD were deposited onto precleaned glass slides in the same manner as described above. GIXD was performed at the Complex Materials Scattering (CMS) beamline of the National Synchrotron Light Source II (NSLS-II), Brookhaven National Laboratory. The X-ray beam with an energy of 13.5 keV shone upon the samples with an incident angle of 0.1° with respect to the substrate, between the critical angles of the P3HT film and the silicon substrate. A custom-made Pilatus-800K detector was placed at 257 mm from the sample center to capture GIWAXS images with the exposure time of 10 s. All GIWAXS images have been background subtracted.

Acknowledgements

This work was supported by ExxonMobil through its membership in the Princeton E-filliates Partnership of the Andlinger Center for Energy and the Environment. K.G. and Y.-L.L. acknowledge support from the National Science Foundation (NSF) through grant CMMI-1824674. Y.W. and R.D.P. acknowledge support from the NSF Materials Research Science and Engineering Center Program through the Princeton Center for Complex Materials (DMR-1420541). C.K.L. acknowledges NSF DMR-1708317. The P3HT samples were synthesized in part upon work supported by the State of Washington through the University of Washington Clean Energy Institute and via funding from the Washington Research Foundation. X-ray scattering measurements were conducted at the Center for Functional Nanomaterials (CFN) and the Complex Materials Scattering (CMS) beamline of the National Synchrotron Light Source II (NSLS-II), which both are U.S. DOE Office of Science Facilities, at Brookhaven National Laboratory under Contract No. DE-SC0012704.

References

- (1) Sirringhaus, H. 25th Anniversary Article: Organic Field-Effect Transistors: The Path beyond Amorphous Silicon. *Adv. Mater.* **2014**, *26*, 1319–1335.
- (2) Dong, H.; Fu, X.; Liu, J.; Wang, Z.; Hu, W. Key Points for High-Mobility Organic Field-Effect Transistors. *Adv. Mater.* **2013**, *25*, 6158–6183.
- (3) Nikolka, M.; Nasrallah, I.; Rose, B.; Ravva, M. K.; Broch, K.; Sadhanala, A.; Harkin, D.; Charmet, J.; Hurhangee, M.; Brown, A.; et al. High Operational and Environmental Stability of High-Mobility Conjugated Polymer Field-Effect Transistors through the Use of Molecular Additives. *Nat. Mater.* **2017**, *16*, 356–362.
- (4) Nikolka, M.; Schweicher, G.; Armitage, J.; Nasrallah, I.; Jellett, C.; Guo, Z.; Hurhangee, M.; Sadhanala, A.; McCulloch, I.; Nielsen, C. B.; et al. Performance Improvements in Conjugated Polymer Devices by Removal of Water-Induced Traps. *Adv. Mater.* **2018**, *30*, 1–8.
- (5) Meng, L.; Zhang, Y.; Wan, X.; Li, C.; Zhang, X.; Wang, Y.; Ke, X.; Xiao, Z.; Ding, L.; Xia, R.; et al. Organic and Solution-Processed Tandem Solar Cells with 17.3% Efficiency. *Science* 2018, 361, 1094–1098.
- (6) Cui, Y.; Yao, H.; Zhang, J.; Xian, K.; Zhang, T.; Hong, L.; Wang, Y.; Xu, Y.; Ma, K.; An, C.; et al. Single-Junction Organic Photovoltaic Cells with Approaching 18% Efficiency. Adv. Mater. 2020, 1908205.
- (7) Tsao, H. N.; Müllen, K. Improving Polymer Transistor Performance via Morphology Control. *Chem. Soc. Rev.* **2010**, *39*, 2372–2386.
- (8) Salleo, A.; Kline, R. J.; DeLongchamp, D. M.; Chabinyc, M. L. Microstructural Characterization and Charge Transport in Thin Films of Conjugated Polymers. *Adv. Mater.* **2010**, *22*, 3812–3838.
- (9) Dang, M. T.; Hirsch, L.; Wantz, G.; Wuest, J. D. Controlling the Morphology and Performance of Bulk Heterojunctions in Solar Cells. Lessons Learned from the Benchmark Poly(3-Hexylthiophene):[6,6]-Phenyl- C61-Butyric Acid Methyl Ester System. *Chem. Rev.* **2013**, *113*, 3734–3765.
- (10) Lee, H.; Park, C.; Sin, D. H.; Park, J. H.; Cho, K. Recent Advances in Morphology Optimization for Organic Photovoltaics. *Adv. Mater.* **2018**, *30*, 1–39.

- (11) Yang, H.; Shin, T. J.; Yang, L.; Cho, K.; Ryu, C. Y.; Bao, Z. Effect of Mesoscale Crystalline Structure on the Field-Effect Mobility of Regioregular Poly(3-Hexyl Thiophene) in Thin-Film Transistors. *Adv. Funct. Mater.* **2005**, *15*, 671–676.
- (12) Clark, J.; Chang, J. F.; Spano, F. C.; Friend, R. H.; Silva, C. Determining Exciton Bandwidth and Film Microstructure in Polythiophene Films Using Linear Absorption Spectroscopy. *Appl. Phys. Lett.* 2009, 94, 2007–2010.
- (13) Aiyar, A. R.; Hong, J. Il; Izumi, J.; Choi, D.; Kleinhenz, N.; Reichmanis, E. Ultrasound-Induced Ordering in Poly(3-Hexylthiophene): Role of Molecular and Process Parameters on Morphology and Charge Transport. ACS Appl. Mater. Interfaces 2013, 5, 2368–2377.
- (14) Zhao, K.; Khan, H. U.; Li, R.; Su, Y.; Amassian, A. Entanglement of Conjugated Polymer Chains Influences Molecular Self-Assembly and Carrier Transport. *Adv. Funct. Mater.* **2013**, *23*, 6024–6035.
- (15) Kleinhenz, N.; Persson, N.; Xue, Z.; Chu, P. H.; Wang, G.; Yuan, Z.; McBride, M. A.; Choi, D.; Grover, M. A.; Reichmanis, E. Ordering of Poly(3-Hexylthiophene) in Solutions and Films: Effects of Fiber Length and Grain Boundaries on Anisotropy and Mobility. *Chem. Mater.* 2016, 28, 3905–3913.
- (16) Surin, M.; Leclère, P.; Lazzaroni, R.; Yuen, J. D.; Wang, G.; Moses, D.; Heeger, A. J.; Cho, S.; Lee, K. Relationship between the Microscopic Morphology and the Charge Transport Properties in Poly(3-Hexylthiophene) Field-Effect Transistors. *J. Appl. Phys.* 2006, 100, 033712.
- (17) Tsao, H. N.; Cho, D.; Andreasen, J. W.; Rouhanipour, A.; Breiby, D. W.; Pisula, W.; Müllen, K. The Influence of Morphology on High-Performance Polymer Field-Effect Transistors. *Adv. Mater.* 2009, 21, 209–212.
- (18) Cho, S.; Lee, K.; Yuen, J.; Wang, G.; Moses, D.; Heeger, A. J.; Surin, M.; Lazzaroni, R. Thermal Annealing-Induced Enhancement of the Field-Effect Mobility of Regioregular Poly(3-Hexylthiophene) Films. J. Appl. Phys. 2006, 100, 114503.
- (19) Vakhshouri, K.; Smith, B. H.; Chan, E. P.; Wang, C.; Salleo, A.; Wang, C.; Hexemer, A.; Gomez, E. D. Signatures of Intracrystallite and Intercrystallite Limitations of Charge Transport in Polythiophenes. *Macromolecules* 2016, 49,

- 7359-7369.
- (20) Katagiri, C.; Nakayama, K. I. Comparison of the Carrier Mobilities of Annealed P3HT Films by Using Charge Carrier Extraction by Linearly Increasing Voltage and Space-Charge Limited Current. *Mol. Cryst. Liq. Cryst.* 2016, 629, 193–199.
- (21) Schulz, G. L.; Ludwigs, S. Controlled Crystallization of Conjugated Polymer Films from Solution and Solvent Vapor for Polymer Electronics. *Adv. Funct. Mater.* **2017**, *27*, 1603083.
- (22) Dingler, C.; Dirnberger, K.; Ludwigs, S. Semiconducting Polymer Spherulites—From Fundamentals to Polymer Electronics. *Macromol. Rapid Commun.* **2019**, *40*, 1–17.
- (23) Chang, J. F.; Clark, J.; Zhao, N.; Sirringhaus, H.; Breiby, D. W.; Andreasen, J. W.; Nielsen, M. M.; Giles, M.; Heeney, M.; McCulloch, I. Molecular-Weight Dependence of Interchain Polaron Delocalization and Exciton Bandwidth in High-Mobility Conjugated Polymers. *Phys. Rev. B* 2006, 74, 115318.
- Ying, L.; Hsu, B. B. Y.; Zhan, H.; Welch, G. C.; Zalar, P.; Perez, L. A.; Kramer, E. J.; Nguyen, T.; Heeger, A. J.; Wong, W.; et al. Regioregular Pyridal[2,1,3]Thiadiazole π-Conjugated Copolymers. *J. Am. Chem. Soc.* 2011, 133, 18538–18541.
- (25) Luo, C.; Ko, A.; Kyaw, K.; Perez, L. A.; Patel, S.; Wang, M.; Grimm, B.; Bazan, G. C.; Kramer, E. J.; Heeger, A. J. General Strategy for Self-Assembly of Highly Oriented Nanocrystalline Semiconducting Polymers with High Mobility. *Nano Lett.* 2014, 14, 2764–2771.
- (26) Zhang, M.; Tsao, H. N.; Pisula, W.; Yang, C.; Mishra, A. K.; Müllen, K. Field-Effect Transistors Based on a Benzothiadiazole-Cyclopentadithiophene Copolymer. J. Am. Chem. Soc. 2007, 129, 3472–3473.
- (27) Himmelberger, S.; Salleo, A. Engineering Semiconducting Polymers for Efficient Charge Transport. *MRS Commun.* **2015**, *5*, 383–395.
- (28) Bronstein, H.; Nielsen, C. B.; Schroeder, B. C.; McCulloch, I. The Role of Chemical Design in the Performance of Organic Semiconductors. *Nat. Rev. Chem.* 2020, 4, 66–77.
- (29) Verploegen, E.; Mondal, R.; Bettinger, C. J.; Sok, S.; Toney, M. F.; Bao, Z.

- Effects of Thermal Annealing upon the Morphology of Polymer-Fullerene Blends. *Adv. Funct. Mater.* **2010**, *20*, 3519–3529.
- (30) Wu, D.; Kaplan, M.; Ro, H. W.; Engmann, S.; Fischer, D. A.; DeLongchamp, D. M.; Richter, L. J.; Gann, E.; Thomsen, L.; McNeill, C. R.; et al. Blade Coating Aligned, High-Performance, Semiconducting-Polymer Transistors. *Chem. Mater.* 2018, 30, 1924–1936.
- (31) Kline, R. J.; McGehee, M. D.; Kadnikova, E. N.; Liu, J.; Fréchet, J. M. J. Controlling the Field-Effect Mobility of Regionegular Polythiophene by Changing the Molecular Weight. *Adv. Mater.* **2003**, *15*, 1519–1522.
- (32) Noriega, R.; Rivnay, J.; Vandewal, K.; Koch, F. P. V; Stingelin, N.; Smith, P.; Toney, M. F.; Salleo, A. A General Relationship between Disorder, Aggregation and Charge Transport in Conjugated Polymers. *Nat. Mater.* **2013**, *12*, 1038–1044.
- (33) Gu, K.; Snyder, C. R.; Onorato, J.; Luscombe, C. K.; Bosse, A. W.; Loo, Y.-L. Assessing the Huang-Brown Description of Tie Chains for Charge Transport in Conjugated Polymers. *ACS Macro Lett.* **2018**, *7*, 1333–1338.
- (34) Qian, Z.; Galuska, L.; McNutt, W. W.; Ocheje, M. U.; He, Y.; Cao, Z.; Zhang, S.; Xu, J.; Hong, K.; Goodman, R. B.; et al. Challenge and Solution of Characterizing Glass Transition Temperature for Conjugated Polymers by Differential Scanning Calorimetry. J. Polym. Sci. Part B Polym. Phys. 2019, 57, 1635–1644.
- (35) Snyder, C. R.; Nieuwendaal, R. C.; DeLongchamp, D. M.; Luscombe, C. K.; Sista, P.; Boyd, S. D. Quantifying Crystallinity in High Molar Mass Poly(3-Hexylthiophene). *Macromolecules* 2014, 47, 3942–3950.
- (36) Merlo, J. A.; Frisbie, C. D. Field Effect Conductance of Conducting Polymer Nanofibers. *J. Polym. Sci. Part B Polym. Phys.* **2003**, *41*, 2674–2680.
- (37) Zhuravlev, E.; Schick, C. Fast Scanning Power Compensated Differential Scanning Nano-Calorimeter: 1. The Device. *Thermochim. Acta* **2010**, *505*, 1–13.
- (38) Mathot, V.; Pyda, M.; Pijpers, T.; Vanden Poel, G.; Van De Kerkhof, E.; Van Herwaarden, S.; Van Herwaarden, F.; Leenaers, A. The Flash DSC 1, a Power Compensation Twin-Type, Chip-Based Fast Scanning Calorimeter (FSC): First Findings on Polymers. *Thermochim. Acta* **2011**, *522*, 36–45.
- (39) Schawe, J. E. K. Influence of Processing Conditions on Polymer Crystallization

- Measured by Fast Scanning DSC. J. Therm. Anal. Calorim. 2014, 116, 1165–1173.
- (40) Sanchez, I. C.; Colson, J. P.; Eby, R. K. Theory and Observations of Polymer Crystal Thickening. *J. Appl. Phys.* **1973**, *44*, 4332–4339.
- (41) Sanchez, I. C.; Peterlin, A.; Eby, R. K.; McCrackin, F. L. Theory of Polymer Crystal Thickening during Annealing. *J. Appl. Phys.* **1974**, *45*, 4216–4219.
- (42) Zen, A.; Saphiannikova, M.; Neher, D. Effect of Molecular Weight on the Structure and Crystallinity of Poly (3-Hexylthiophene). *Macromolecules* **2006**, *39*, 2162–2171.
- (43) Koch, F. P. V.; Rivnay, J.; Foster, S.; Müller, C.; Downing, J. M.; Buchaca-Domingo, E.; Westacott, P.; Yu, L.; Yuan, M.; Baklar, M.; et al. The Impact of Molecular Weight on Microstructure and Charge Transport in Semicrystalline Polymer Semiconductors-Poly(3-Hexylthiophene), a Model Study. *Prog. Polym. Sci.* 2013, 38, 1978–1989.
- (44) Mollinger, S. A.; Krajina, B. A.; Noriega, R.; Salleo, A.; Spakowitz, A. J. Percolation, Tie-Molecules, and the Microstructural Determinants of Charge Transport in Semicrystalline Conjugated Polymers. ACS Macro Lett. 2015, 4, 708–712.
- (45) Baker, J. L.; Jimison, L. H.; Mannsfeld, S.; Volkman, S.; Yin, S.; Subramanian, V.; Salleo, A.; Alivisatos, A. P.; Toney, M. F. Quantification of Thin Film Crystallographic Orientation Using X-Ray Diffraction with an Area Detector. *Langmuir* **2010**, *26*, 9146–9151.
- (46) Sirringhaus, H.; Brown, P. J.; Friend, R. H.; Nielsen, M. M.; Bechgaard, K.; Langeveld-Voss, B. M. W.; Spiering, a. J. H.; Janssen, R. a. J.; Meijer, E. W.; Herwig, P.; et al. Two-Dimensional Charge Transport in Self-Organized, High-Mobility Conjugated Polymers. *Nature* **1999**, *401*, 685–688.
- (47) Salleo, A. Charge Transport in Polymeric Transistors. *Mater. Today* **2007**, *10*, 38–45.
- (48) Brinkmann, M. Structure and Morphology Control in Thin Films of Regioregular Poly(3-Hexylthiophene). *J. Polym. Sci. Part B Polym. Phys.* **2011**, *49*, 1218–1233.
- (49) Turner, S. T.; Pingel, P.; Steyrleuthner, R.; Crossland, E. J. W.; Ludwigs, S.; Neher, D. Quantitative Analysis of Bulk Heterojunction Films Using Linear

- Absorption Spectroscopy and Solar Cell Performance. *Adv. Funct. Mater.* **2011**, 21, 4640–4652.
- (50) Gierschner, J.; Huang, Y.; Averbeke, B. Van; Cornil, J.; Friend, R. H.; Beljonne, D. Excitonic versus Electronic Couplings in Molecular Assemblies: The Importance of Non-Nearest Neighbor Interactions. *J. Chem. Phys.* 2009, 130, 044105.
- (51) Lu, G.; Blakesley, J.; Himmelberger, S.; Pingel, P.; Frisch, J.; Lieberwirth, I.; Salzmann, I.; Oehzelt, M.; Di Pietro, R.; Salleo, A.; et al. Moderate Doping Leads to High Performance of Semiconductor/Insulator Polymer Blend Transistors. *Nat. Commun.* 2013, 4, 1588.
- (52) Huang, Y.-L.; Brown, N. The Effect of Molecular Weight on Slow Crack Growth in Linear Polyethylene Homopolymers. *J. Mater. Sci.* **1988**, *23*, 3648–3655.
- (53) Hoffman, J. D.; Miller, R. L. Kinetic of Crystallization from the Melt and Chain Folding in Polyethylene Fractions Revisited: Theory and Experiment. *Polymer* (Guildf). 1997, 38, 3151–3212.
- (54) Ferrer-Balas, D.; Maspoch, M. L.; Martinez, A. B.; Santana, O. O. Influence of Annealing on the Microstructural, Tensile and Fracture Properties of Polypropylene Films. *Polymer (Guildf)*. 2001, 42, 1697–1705.
- (55) Segatta, F.; Lattanzi, G.; Faccioli, P. Predicting Charge Mobility of Organic Semiconductors with Complex Morphology. *Macromolecules* **2018**, *51*, 9060–9068.
- (56) Certain Commercial Equipment, Instruments, or Materials Are Identified in This Paper in Order to Specify the Experimental Procedure Adequately. Such Identification Is Not Intended to Imply Recommendation or Endorsement by the National Institute of Standar.
- (57) Bronstein, H. A.; Luscombe, C. K. Externally Initiated Regioregular P3HT with Controlled Molecular Weight and Narrow Polydispersity. *J. Am. Chem. Soc.* **2009**, *131*, 12894–12895.
- (58) Gu, K.; Onorato, J.; Xiao, S. S.; Luscombe, C. K.; Loo, Y.-L. Determination of the Molecular Weight of Conjugated Polymers with Diffusion-Ordered NMR Spectroscopy. *Chem. Mater.* 2018, 30, 570–576.

(59) Treviño-Quintanilla, C. D.; Krishnamoorti, R.; Bonilla-Ríos, J. Flash DSC Crystallization Study for Blown Film Grade Bimodal HDPE Resins. I. Isothermal Kinetics and Its Application of the Blown Film Modeling. *J. Polym. Sci. Part B Polym. Phys.* 2016, 54, 2425–2431.

Supporting figures

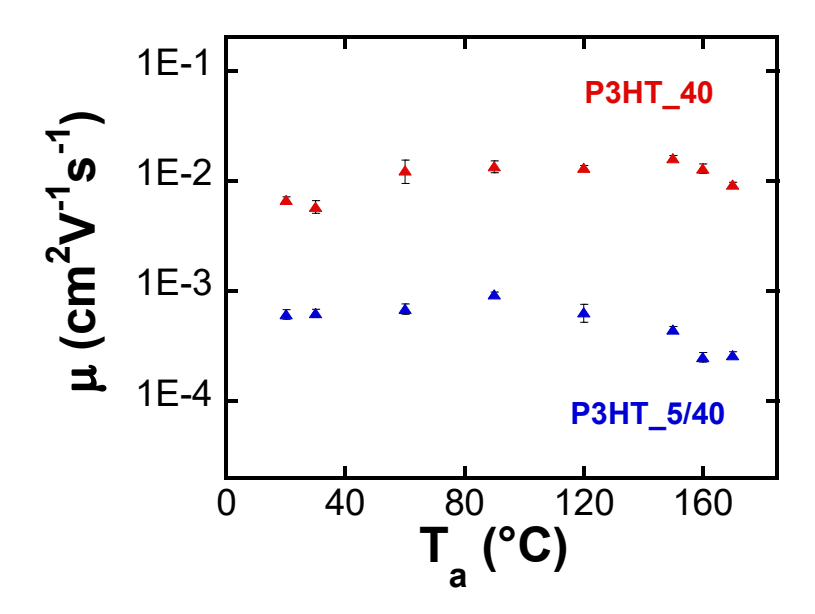


Figure S1. The field-effect mobility of transistors comprising P3HT _40 and P3HT_5/40 films that had been annealed at different temperatures.

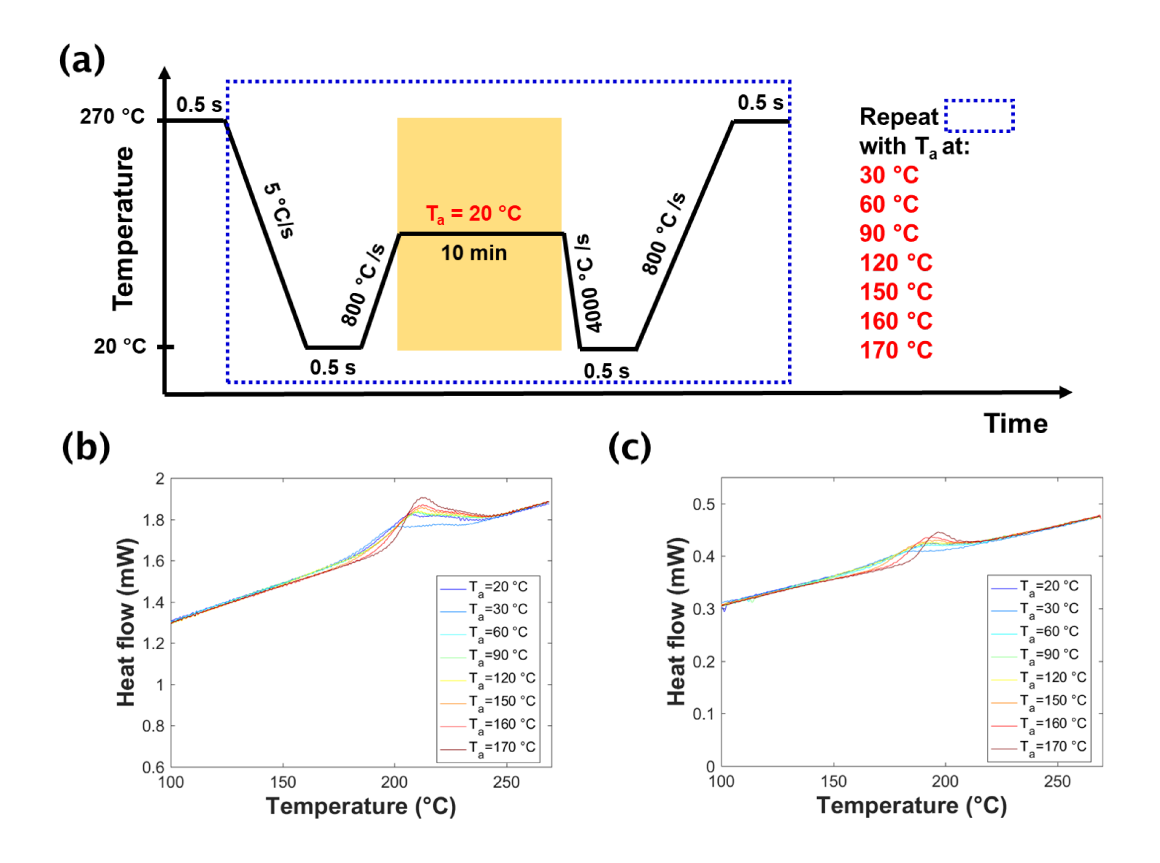


Figure S2. (a) Thermal history to investigate the dependence of thermal properties of P3HT on cooling rates with flash-DSC. The cooling rates ranged from 4000 °C/s to 0.16 °C/s. (b) Flash-DSC thermograms of P3HT_40 that had been annealed at different temperatures. (c) Flash-DSC thermograms of P3HT_5/40 that had been annealed at different temperatures.

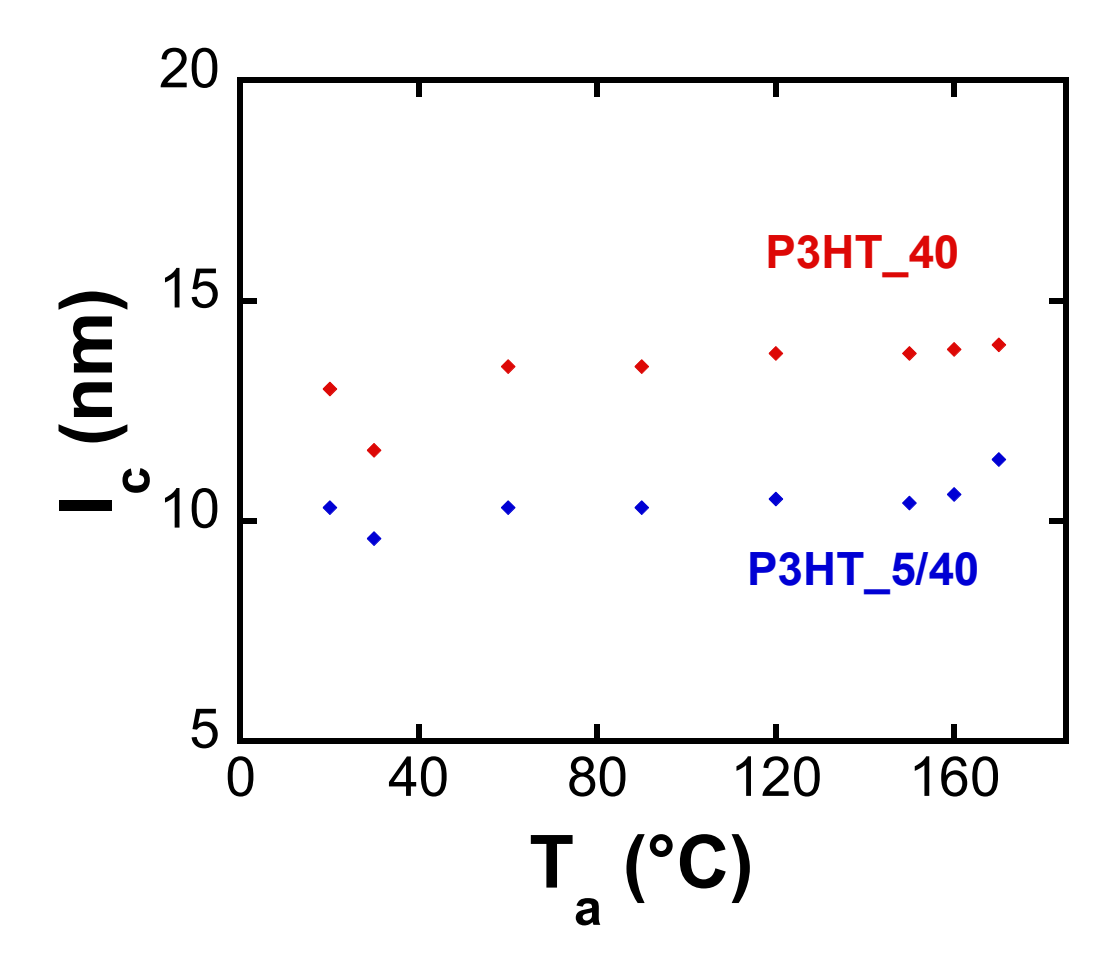


Figure S3. Crystallite thickness, as determined from the melting temperature, of P3HT_40 and P3TH_5/40 as a function of annealing temperature.

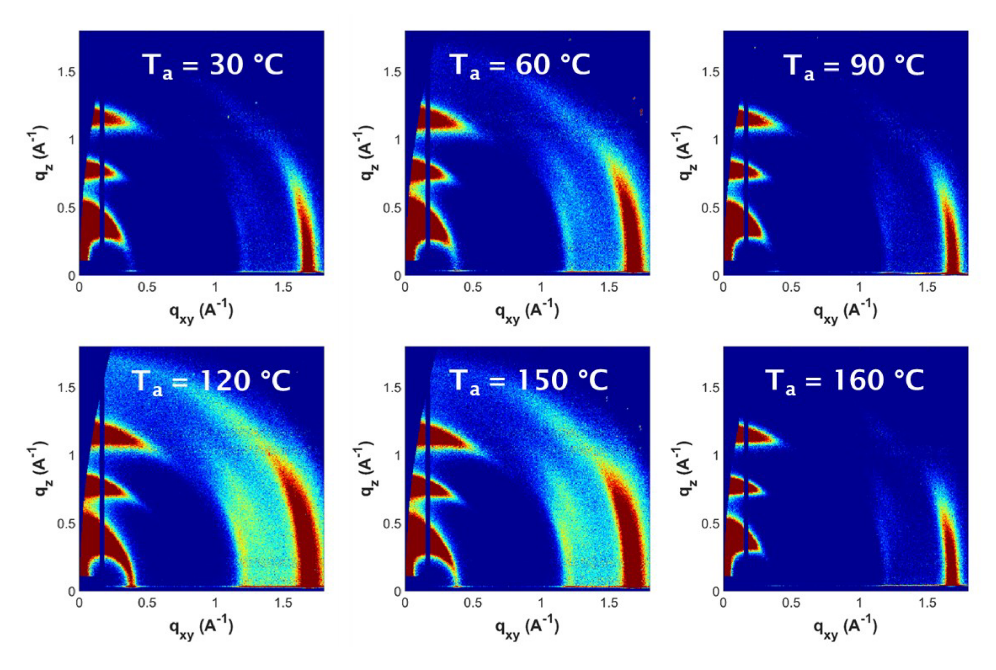


Figure S4. 2D GIXD pattern of P3HT_40 thin films that had been annealed at different temperatures acquired at room temperature.

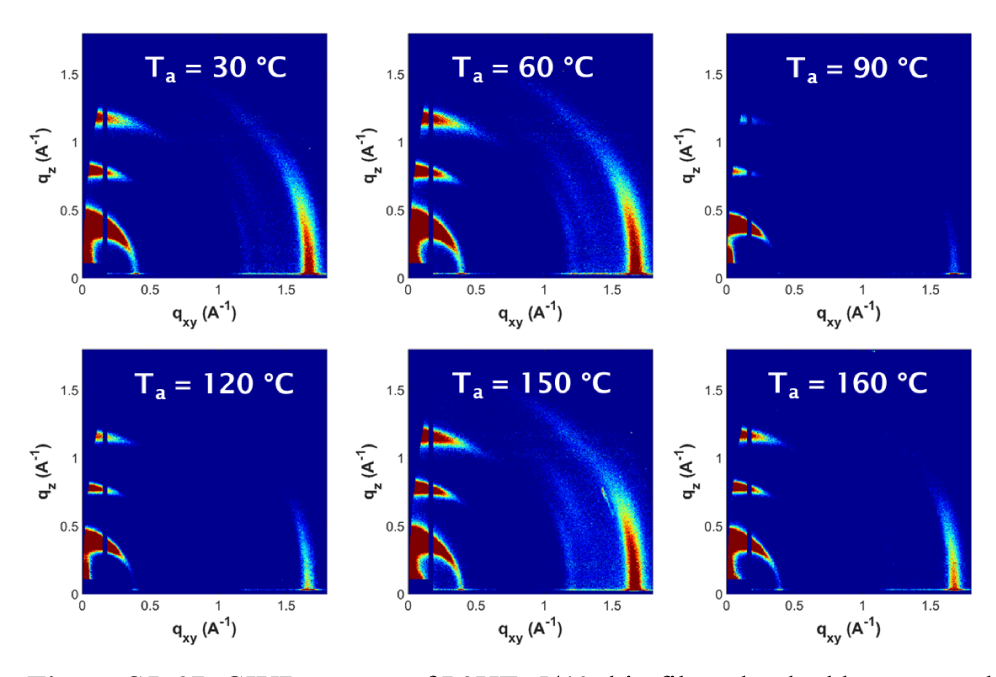


Figure S5. 2D GIXD pattern of P3HT_5/40 thin films that had been annealed at different temperatures acquired at room temperature.